



In Silico Structural Modeling and Analysis of Physicochemical Properties of Antitumoral QS-13 Peptide and Its Derivatives in Water and Dimethyl Sulfoxide

Vivien Paturel, Stéphanie Baud, Christophe Schneider, Sylvie Brassart-pasco

► To cite this version:

Vivien Paturel, Stéphanie Baud, Christophe Schneider, Sylvie Brassart-pasco. In Silico Structural Modeling and Analysis of Physicochemical Properties of Antitumoral QS-13 Peptide and Its Derivatives in Water and Dimethyl Sulfoxide. *Peptide Science*, 2024, 116 (5), pp.e24352. <10.1002/pep2.24352>. <hal-04746194>

HAL Id: hal-04746194

<https://hal.science/hal-04746194v1>

Submitted on 21 Oct 2024

HAL is a multi-disciplinary open access archive for the deposit and dissemination of scientific research documents, whether they are published or not. The documents may come from teaching and research institutions in France or abroad, or from public or private research centers.

L'archive ouverte pluridisciplinaire **HAL**, est destinée au dépôt et à la diffusion de documents scientifiques de niveau recherche, publiés ou non, émanant des établissements d'enseignement et de recherche français ou étrangers, des laboratoires publics ou privés.



Distributed under a Creative Commons CC BY 4.0 - Attribution - International License

ARTICLE OPEN ACCESS

In Silico Structural Modeling and Analysis of Physicochemical Properties of Antitumoral QS-13 Peptide and Its Derivatives in Water and Dimethyl Sulfoxide

Vivien Paturel¹ | Stéphanie Baud^{1,2} | Christophe Schneider¹ | Sylvie Brassart-Pasco¹

¹UMR 7369 Matrice Extracellulaire et Dynamique Cellulaire (MEDyC), CNRS, Université de Reims Champagne Ardenne, Reims, France | ²Plateau de Modélisation Moléculaire Multi-échelle (P3M), Université de Reims Champagne Ardenne, Reims, France

Correspondence: Sylvie Brassart-Pasco (sylvie.brassart-pasco@univ-reims.fr)

Received: 25 January 2024 | **Revised:** 7 May 2024 | **Accepted:** 9 May 2024

Funding: This work was supported by the Région Champagne-Ardenne, the Université de Reims Champagne Ardenne, the Ligue Contre le Cancer (Conférence de Coordination Inter Régionale du Grand Est: CCIR-GE), the Centre Nationale de la Recherche Scientifique and ITMO Cancer of Aviesan. Vivien Paturel is a PhD fellow funded by Région Champagne-Ardenne and Université de Reims Champagne Ardenne.

Keywords: collagen IV | DMSO | QS-13 | secondary structure | solubility | tetrastatin

ABSTRACT

The NC1 domain of the alpha 4 chain of type IV collagen was previously reported to exert anti-tumor properties in a melanoma model and to inhibit angiogenesis. The minimal active sequence identified to date comprises 13 amino acids: QKISRCQVCVKYS. Unfortunately, this sequence is not soluble in aqueous media and requires prior dissolution in DMSO. The disulfide bridge (DB) that spontaneously forms in solution between two cysteine residues is crucial for its biological activity. The aim of this article was to study the impact of DMSO on the physicochemical properties of the QS-13 peptide and to replace hydrophobic amino acids to enhance its water solubility. Using bioinformatics (GROMACS, VMD, and ProtParam) and programming (Python and RStudio) software programs, we demonstrated that DMSO could promote the formation of DBs, but it is not strictly necessary. Among the QS-13 substituted peptides, some were demonstrated to display similar characteristics to the original peptide. Improved water solubility will make the peptide easier to use in biological studies and facilitate its administration for potential therapeutic applications.

1 | Introduction

Collagen IV, an essential component of the extracellular matrix (ECM), plays a crucial role in maintaining tissue integrity and regulating cellular behavior. Its diverse functions go beyond simple structural support, as it actively participates in cellular signaling processes. The NC1 domain of the $\alpha 4(\text{IV})$ collagen chain was previously demonstrated to inhibit melanoma progression [1]. The minimal active sequence identified to date comprises 13 amino acids, QKISRCQVCVKYS (QS-13), and binds to melanoma cells

through $\alpha v\beta 3$ integrin. The binding site is located in close vicinity to the RGD binding site. QS-13 interaction with $\alpha v\beta 3$ integrin inhibits the FAK/PI3K/Akt pathway, a transduction pathway that is largely involved in tumor cell proliferation and migration. The presence of a disulfide bridge (DB) between the two cysteine residues is crucial for cell binding [2]. QS-13 peptide was also reported inhibiting angiogenesis in vitro through $\alpha v\beta 3$ and $\alpha 5\beta 1$ integrin binding on endothelial cells and in vivo in a Matrigel plug assay [3]. Unfortunately, the QS-13 peptide is currently not soluble in water and requires prior dissolution in dimethyl sulfoxide (DMSO).

The last two authors contributed equally to this study.

The first two authors are co-first authors.

This is an open access article under the terms of the [Creative Commons Attribution](https://creativecommons.org/licenses/by/4.0/) License, which permits use, distribution and reproduction in any medium, provided the original work is properly cited.

© 2024 The Author(s). *Peptide Science* published by Wiley Periodicals LLC.

DMSO is known for its catalytic effect on the formation of DBs between cysteine residues [4]. The literature also reports that DMSO has a significant impact on various cellular processes, especially those related to cancer, as it induces numerous changes in macromolecule secondary structures, which may affect experimental outcomes, even at very low concentrations [4]. Therefore, to further study this peptide, it is necessary to understand the impact of DMSO on the formation of DBs within this peptide. For this purpose, we will model the original QS-13 peptide in two distinct environments, namely water and DMSO. This approach will allow us to explore the solvent's impact on the proximity of sulfur atoms, thereby considering the potential increase in the likelihood of DB formation.

Molecular dynamics (MD) of biological systems is generally conducted in water, with co-solvents considered on the sidelines. Although some models such as DMSO, octane, and ethanol [5–8] exist, they are not as commonly used as water [9]. Studying the three-dimensional structure of QS-13 in different solvents provides information on its conformational stability and thus the possible modulation of its potential interactions with a target molecule. Using MD, we propose to observe trends in bringing the sulfur atoms of cysteine residues closer together and, consequently, opportunities for DB formation.

Given that solubilization is initially achieved at 100% in DMSO in our biological experiments, our methodological approach aims to develop a simulation box model consisting exclusively of DMSO or, alternatively, exclusively of water. This strategy allowed us to explore behaviors at both ends of the spectrum, represented by simulation environments comprising 100% DMSO and 100% water, respectively. Consequently, this study is not only innovative but also contributes to the scientific literature on peptide simulations in DMSO, a solvent frequently used in biology to dissolve peptides insoluble in water. By examining specific molecular interactions in this specific environment, our work aims to enhance existing knowledge and broaden perspectives for a more effective and precise use of DMSO in biomolecular studies.

The relationship between the three-dimensional structure of peptides and their biological function is a fundamental aspect of molecular biochemistry. The spatial conformation of peptides, guided by their specific amino acid sequence, determines their ability to selectively interact with other biological molecules (proteins, lipids, or nucleic acids). This three-dimensional architecture directly influences molecular recognition and binding to cellular receptors, thereby regulating numerous biological processes. Sforça et al. reported that eumenine mastoparan-AF(INLLKIAKGIIKSL-NH₂, EMP-AF-NH₂), isolated from solitary wasp venom, has a more potent biological activity than its analogue containing a carboxyl-free C-terminus, INLLKIAKGIIKSL-COO-(EMP-AF-COO-); besides the expected reduction of its positive charge, the presence of the free carboxyl group at C-terminus introduces a local molecular instability that is able to partly destabilize not only the hydrogen bond pattern of that stretch of helix but also the peptide as a whole [10]. Structural motifs such as helices, beta sheets, and turns play a crucial role in the stability and specificity of interactions, enabling peptides to fulfill various roles, from cellular

signaling to enzymatic modulation. Spatial conformation would be even more critical for interactions, and even more important than the chemical composition of the sequence [11–13].

In the second part of the present article, we will investigate the folding of the peptide by analyzing the distance between the alpha carbons at the C-terminal and N-terminal, induced by the presence of DMSO using the GROMACS algorithm suite [14, 15]. An in-depth study of the peptide's three-dimensional structure under the influence of DMSO will also be conducted, both on a global scale and at the level of each residue, using the DSSP (Define Secondary Structure of Proteins) algorithm [16].

As previously undertaken by other research teams, our final aim will be to modify the peptidic sequence of QS-13 by substituting hydrophobic amino acids with hydrophilic ones [17]. To achieve this, we will replace these amino acids with others bearing a strong resemblance to the initial amino acids in terms of steric hindrance and charge, using the available computational method from the ExPASy Server [18]. In particular, such modifications can be based on the use of amino acid substitution matrices [19].

Then, we will perform an analysis of the hydrophobicity profiles of the resulting peptides, using ProtParam [18]. Additionally, we will analyze their ability to bring sulfur atoms closer together in water, as well as their end-to-end distances (EED) to select peptides most similar to the original QS-13. Simultaneously, we will conduct a thorough analysis of the overall and residue-specific three-dimensional structures of these modified peptides, highlighting the relationship between structure and function. To validate our computational simulations, we will perform a Ramachandran plot [20] to ensure that torsion angles do not lead to aberrant conformations. Finally, clustering will be executed to visualize the predominant conformations of each generated peptide, constituting a crucial step in the section dedicated to amino acid substitution.

2 | Materials and Methods

2.1 | Peptide Modeling Without DB

The five modified peptides, along with the original QS-13, were modeled in an extended conformation using the Molefacture extension of the Visual Molecular Dynamics (VMD) software [21]. The peptides were then capped with N-ter (NT2) and C-ter (ACE), using the AutoPSF extension of VMD. The following MD simulations were performed using the GROMACS software (version 2020.1) [14] and the OPLSAA (Optimized Potentials for Liquid Simulations All-Atom) [22] force field to model the molecular interactions.

Each peptide was solvated in the presence of counterions, an essential step to enable MD under neutral charge conditions. Water was described using the TIP3P model [23], ensuring a suitable environment for studying molecular interactions under physiological conditions. Regarding solvation in DMSO, based on existing parameters in the OPLSAA forcefield [23], the DMSO topology was constructed.

All structures were submitted to an energy minimization process to obtain an initial balanced molecular conformation. A maximum of 50,000 steps of the steepest descent algorithm were used with a minimum energy tolerance of 1000.0 kJ/mol/nm and a maximum displacement step set to 0.01 nm.

The systems were then equilibrated in two phases. First, an NVT (Number of Particles, Volume, Temperature) ensemble simulation was conducted for 160 ps. Initial velocities were generated using a Maxwell distribution with a reference temperature of 310 K. The leap-frog integration algorithm was employed with a time step of 0.002 ps (2 fs) as hydrogen bonds were constrained using the LINCS algorithm [24]. Temperature coupling was achieved using the V-rescale thermostat [25] with a time constant of 0.1 ps and a reference temperature of 310 K for both protein and nonprotein groups. Nonbonded interactions were calculated with a Coulomb cutoff of 1.0 nm and a van der Waals cutoff of 1.0 nm. Long-range electrostatics were handled using the Particle Mesh Ewald (PME) [26] method. Subsequently, an NPT ensemble simulation was performed for 160 ps to equilibrate the system at specific pressure and temperature conditions. In addition to the temperature V-rescale coupling, pressure coupling was performed using the Parrinello–Rahman algorithm [27] with a time constant of 2.0 ps and a reference pressure of 1.0 bar. The integration parameters, bond constraints, nonbonded interactions, and electrostatics conditions were similar to those in the NVT simulation. Finally, NPT production runs were performed for 100 ns. Given the size of the peptides considered, the intrinsically comparative nature of the study carried out, and the previous expertise acquired in connection with the study of matrikines [2, 28–30], this sampling time is appropriate. This is all the more so as the data extracted from the present simulations and linked to canonical peptides are in agreement with those obtained previously [2]. Both during equilibration and production processes, periodic boundary conditions were applied in all three dimensions and coordinates, velocities, and energies were saved every 1.0 ps.

2.2 | Peptide Modeling with DB

The initial structures for MD simulations were selected as follows: MD simulations of peptides without DB were monitored by computing the distance between the sulfur atoms of the cysteine residues along the trajectory. The structures corresponding to the smallest distance (as presented in Table 1) were then selected and used to generate structures containing the DB. From the obtained starting conformations, MD simulations were then performed following the protocol described above.

2.3 | Measurement of SSD (Sulfur-to-Sulfur Distances) and EED

GROMACS 2020.1 software and more particularly the distance module was used to measure both the distances between the sulfur atoms of the two cysteine residues and the EED. The EED was defined as the distance between the alpha carbon atoms of the glutamine (N-ter) and serine (C-ter) residues. This consistent approach provided insights into both the distances between the sulfur atoms of cysteines and, consequently, the potential likelihood of spontaneous DB formation, as well as the EED allowing us to evaluate the folding of the peptide.

The time evolution of EED and SSD was smoothed and plotted using a sliding window of 50 ps, over which distances were averaged to avoid abrupt fluctuations.

2.4 | Distances Data Distributions

The RStudio software was employed to process the generated data and create various distributions along with corresponding panels. The data were utilized for all measurements, encompassing the full set of conformations throughout the MD (10,001 conformations per peptide, equivalent to 100 ns of MD). Subsequently, the distances were categorized into intervals of 0.05 nm, representing the number of conformations (occurrences per interval) within each 0.05-nm slice.

2.5 | Averaged and Per Residue Secondary Structure

The simulations were processed via the DSSP function available in GROMACS 2020.1, and the extracted data were then processed with a home written script. The DSSP function implements the DSSP [16] algorithm and allows the analysis of the secondary structure of peptides. For each simulation, both with and without DBs in the peptides, we performed DSSP analysis on the entire 100-ns trajectory. This allowed us to examine the secondary structure characteristics throughout the simulation time. We investigated the DSSP results on two levels: the secondary structure averaged along the peptide sequence and the local secondary structure content explored by each residue. By considering the global secondary structure of the peptides, we gained insights into the conformational stability and folding patterns. Additionally, analyzing the secondary structure on a residue-by-residue basis provided detailed information on local structural variations and potential regions of interest.

TABLE 1 | Representative table of sequences of QS-13 derivatives and minimum distances between sulfur atoms during 100 ns of molecular dynamics.

Peptide	Distance between sulfur atoms of the cysteine (nm)	Sequence
QS-13-1	0.353	QKSSRCQVCVKYS
QS-13-2	0.342	QKSSRCQGCGKYS
QS-13-3	0.354	QKGSRCQGCVKYS
QS-13-4	0.355	QKGSRCQGCGKYS
QS-13-5	0.344	QKGSRCQGCSKYS

2.6 | Physicochemical Parameters Analysis

A set of physicochemical parameters of the different peptides were predicted using the ProtParam tool of ExPASy (<https://web.expasy.org/protparam/>) [18]: namely, molecular weight, extinction coefficients, estimated half-life, instability index, and GRAVY (Grand Average of Hydropathicity index). The GRAVY value for a peptide or protein is calculated as the sum of the [hydropathy values](#) [31] of all the amino acids, divided by the number of residues in the sequence. A peptide or a protein is considered water-soluble when the associated GRAVY value is lower than 0, because in that case the molecule is hydrophilic. Isoleucine and valine residues from QS-13 (QKISRCQVCVKYS) were replaced with glycine and serine residues. These substitutions were tested using ProtParam [18] to examine their stability (which should be below 40), their charges (matching QS-13, i.e., +3), and their hydropathicity.

2.7 | Ramachandran Diagrams Generation

Ramachandran diagrams were generated for each peptide and over the entire 100-ns simulation using the rama tool of the GROMACS software. Subsequently, a home written Python script was utilized to plot the obtained results. This script performs analysis and visualization of Ramachandran plots, which are used to explore the distribution of phi (ϕ) and psi (ψ) dihedral angles in protein structures. The script's functionality uses two libraries: NumPy for numerical computations and Matplotlib.pyplot for creating plots.

2.8 | Clustering

The conformations of the trajectories were clustered based on the positions of the alpha carbons both in the original QS-13 peptide and its derivatives. This operation was carried out using the GROMACS software, employing the gromos algorithm. The chosen cutoff criterion to distinguish the different families was set to 3 Å. This clustering approach allowed us to define clusters [32] and thus to identify the main conformations explored by the investigated peptides.

2.9 | Visualization of Peptides

In this study, graphical representations were generated using VMD [21]. The protein backbone was depicted in cartoon representation, while the side chains were shown in licorice representation without the hydrogen atoms. Additionally, the alpha carbons in the glutamine (N-ter) and serine (C-ter) were visualized in van der Waals view, with the C-terminus displayed in green and the N-terminus in red.

2.10 | Graphical Representation

The graphical representation of the obtained results was carried out using Python3, specifically the Matplotlib.pyplot module, as well as GraphPad Prism 9.0.0.

2.11 | Peptide Solubility Assessment

The original QS-13 and the QS-13-3 peptides were synthesized by Proteogenix (Schiltigheim, France). The original QS-13 was either pre-dissolved in DMSO (20 mM stock solution in DMSO) or directly solubilized in the culture medium (DMEM Gibco 4.5 g/L glucose). QS-13-3 was directly dissolved in the culture medium. The final concentration was 40 μ M for each peptide. One milliliter of peptide solution was added per well of a six-well plate and the images were acquired after a 2-h incubation at 37°C using IncuCyte S3 (4× objective).

2.12 | Migration Assay

HT144 melanoma cells, purchased from ATCC (HTB-63), were seeded in 96-well Imagelock plates (for IncuCyte) at a density of 45,000 cells per well and incubated overnight in DMEM containing 10% fetal bovine serum (FBS). An open wound area was created in the cell monolayer using the IncuCyte Wound Maker tool. Cells were washed with PBS, and then incubated with DMEM alone as a control or with QS-13 and QS-13-3 peptides at a concentration of 40 μ M. Wound closure was monitored for 16 h. Statistical analysis was conducted using a Student's *t*-test. Additionally, graphics representing the migration slopes of the various experimental conditions were generated between the 4- and 16-h incubation periods. Images were acquired using the IncuCyte S3, and analyses were performed with the wound healing analysis module. The images show the confluence mask in purple and the initial wound area in red. These results represent two independent experiments with $n=8$ biological replicates, * $p < 0.05$, ** $p < 0.01$ using a Student's *t*-test.

3 | Results

3.1 | Influence of Solvent on QS-13 Peptide Structure

We were first interested in the distance between sulfur atoms from the cysteine residues in the QS-13 peptide in DMSO (-d) and water (-w). As a reference, we first determined the average distance between sulfur atoms from the cysteine residues in the QS-13 peptide with a constrained DB (-DB), over a 100-ns simulation, in a DMSO box, (Table 2 and Figure 1). The average

TABLE 2 | DMSO promotes shorter distances between sulfur atoms and thus could favor the formation of disulfide bonds between the cysteine residues by bringing them closer.

SSD	Average distance (nm)	Standard deviation (nm)
QS-13-w	0.926	0.235
QS-13-d	0.825	0.189
QS-13-DB-d	0.204	0.004

Note: Measurement of distances between sulfur atoms of the cysteine residues was performed using the gmx distance from GROMACS along the 100 ns of simulation.

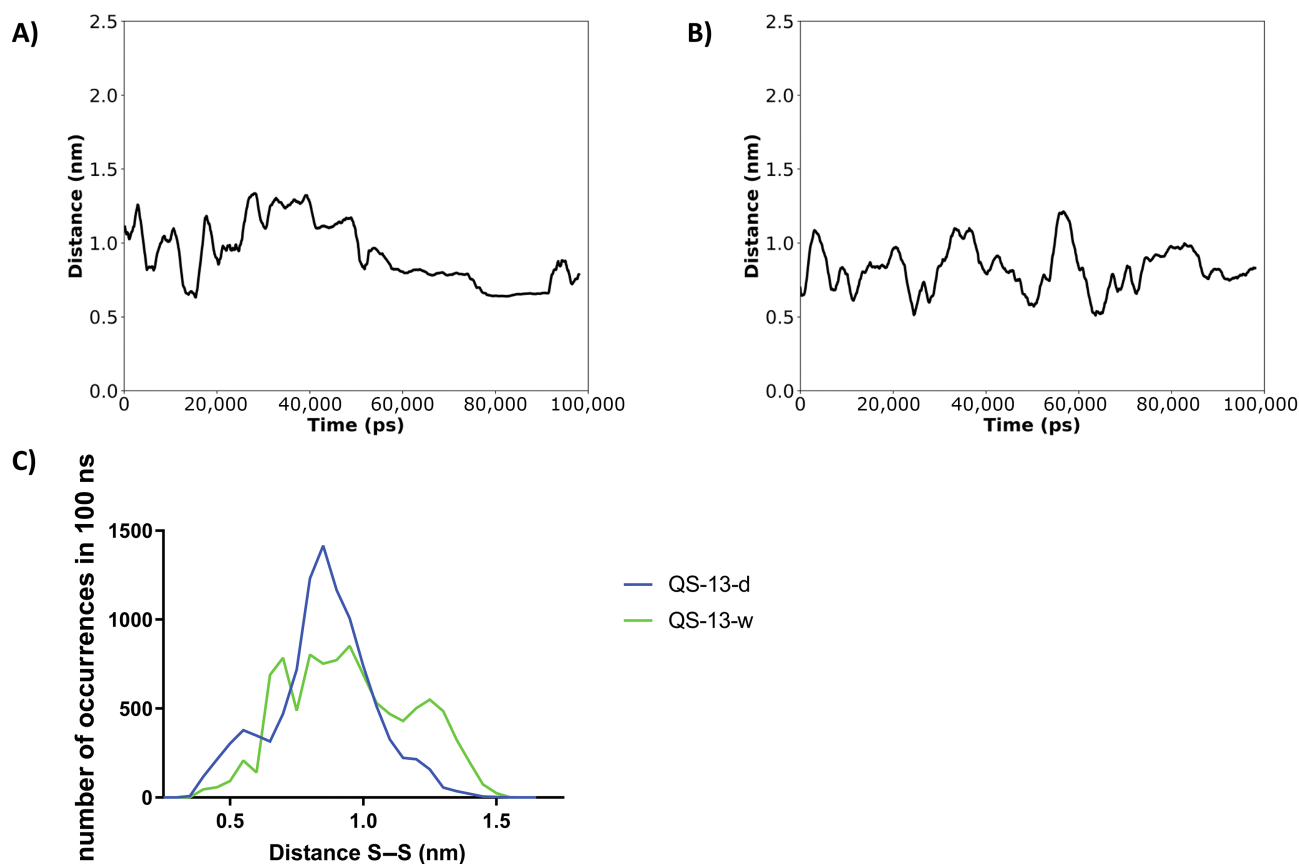


FIGURE 1 | Influence of solvent on the distance between cysteine residues in the QS-13 peptide. (A) Time evolution of the distance between sulfur atoms from the cysteine residues of the QS-13 peptide in water (QS-13-w). (B) Time evolution of the distance between sulfur atoms from the cysteine residues of the QS-13 peptide in DMSO (QS-13-d). (C) Occurrences according to sulfur atom distances. Values were obtained using a script on RStudio, with an interval of 0.05 nm.

distance between the sulfur atoms of the cysteine residues in QS-13-d was 0.825 ± 0.189 nm. In QS-13-w, the average distance is greater (0.926 ± 0.235 nm). DMSO promotes shorter distances between sulfur atoms and may favor the formation of disulfide bonds between the cysteine residues by bringing them closer.

We then focused on the distance between glutamine (N-ter) and serine (C-ter) residues in the two solvents to characterize the solvent impact on QS-13 shape and folding. Table 3 and Figure 2 show, respectively, the time evolutions and the average values of the distance between the alpha carbons of the glutamine and serine residues in each solvent (DMSO and water). Again, the peptide simulated in DMSO and containing a DB (QS-13-DB-d) is considered as a reference. For this peptide, the observed average distance is equal to 2.600 ± 0.441 nm. The average distances in QS-13-d and QS-13-w were 2.296 ± 0.414 and 1.307 ± 0.516 nm, respectively. These results suggest that the QS-13-d behaves the same way as the QS-13-DB-d and is less “folded” than the QS-13-w.

The distances between the alpha carbons of the glutamine and serine residues as a function of time for the QS-13-w, QS-13-d, and QS-13-DB-d are reported in Figure 2A, B, and C, respectively. As above, the behavior of QS-13-d is very similar to QS-13-DB-d (Figure 2B,C). In QS-13-w, the N-ter and C-ter ends tend to come closer than in QS-13-d, with a pick around 1 nm (Figure 2A). In the presence or absence of the DB, QS-13 presents very similar distance distribution profiles (Figure 2D);

TABLE 3 | Water brings the ends of QS-13 closer.

EED	Average distance (nm)	Standard deviation (nm)
QS-13-w	1.307	0.516
QS-13-d	2.296	0.414
QS-13-DB-d	2.600	0.441

Note: Measurement of distances between the alpha carbon of glutamine and serine using the gmxdistance from GROMACS along the 100 ns of simulation.

only a slight shift to the right is observed upon the creation of the DB.

The effect of the solvent on the secondary structure was then investigated in two ways: first, the global content of different secondary structures per peptide was averaged over the whole trajectories (Figure 3A–C), and second, a more local analysis was performed focusing on the local secondary structure explored by each residue along the peptide (Figure 3D–F). The three major local secondary structures adopted by QS-13-w are coils, bends, and turns. Helices are also explored in a small proportion (Figure 3A). QS-13-d peptide explored only coils and bends local secondary structures (Figure 3B). The proportion of turns is drastically decreased compared with QS-13-w. The presence of a DB in DMSO (QS-13-DB-d) favored coils and bends but also promoted turns and the 3_{10} helix (Figure 3C).

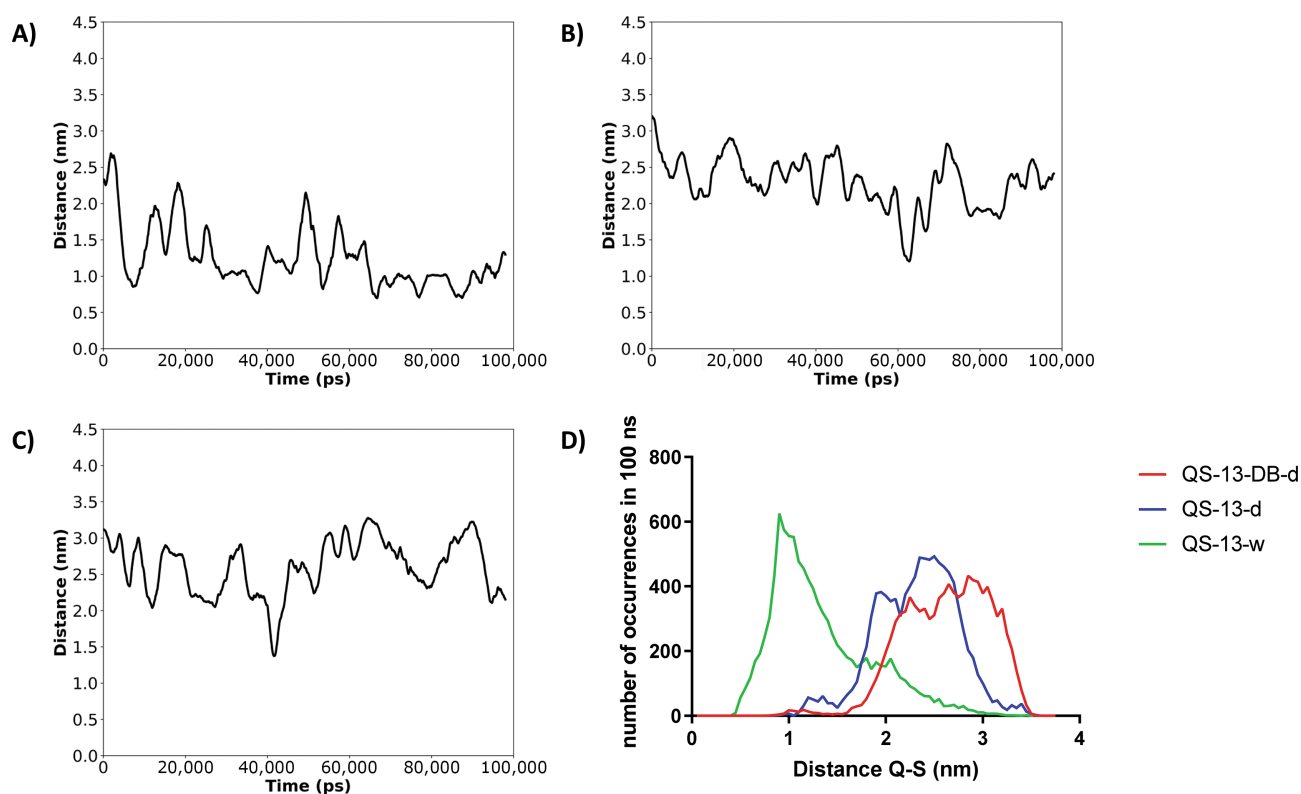


FIGURE 2 | Influence of solvent on the distance between the alpha carbons of the glutamine and serine residues of the QS-13 peptide. (A) Time evolution of the distance between the alpha carbons of the glutamine and serine residues of the QS-13-w. (B) Time evolution of the distance between the alpha carbons of the glutamine and serine residues of the QS-13-d. (C) Distance between the alpha carbons of the glutamine and serine residues of the QS-13-DB-d. (D) Occurrences according to distance between the alpha carbons of the glutamine and serine residues. Values were obtained with a script on RStudio, with an interval of 0.05 nm.

In addition, for each peptide, the local secondary structure adopted by each residue of the QS-13 peptides was assessed (Figure 3D–F). Globally, it was observed that the C-ter and N-ter parts of the peptide tend to explore coil conformations (in gray). The central residues adopted a bend shape with QS-13-DB-d (Figure 3F) (in blue), and half bend half coil for QS-13-d (Figure 3E). Finally, Figure 3D highlights that for QS-13-w, QS-13 has an helix and turn conformation (brown and orange, respectively). It should be noted that the DB increases the bend conformation between the cysteine residues.

3.2 | Hydrophobic Amino Acids Substitutions and Consequences on Peptide Physicochemical Parameters and Structure

The aim of this part was to substitute hydrophobic amino acids within the QS-13 sequence to increase its solubility, without impacting too much its stability and other physicochemical parameters.

The physicochemical parameters of the substituted peptides are reported in Table 4. It can be observed that the suggested substitutions do not modify the pI, the charge, or the estimated half-life. All substituted peptides present a stability index below 40, which indicates that they should be stable in solution (peptide stability: QS-13 > QS-13-4 > QS-13-5 > QS-13-1 > QS-13-3 > QS-13-2) (Figure 4A). They should be more soluble than the QS-13

peptide as their hydrophily indexes are smaller (< -0.75) (peptide solubility in water: QS-13-2 > QS-13-5 > QS-13-4 > QS-13-3 > QS-13-1 > QS-13) (Figure 4B).

We then focused on the structural properties of the above substituted peptides. We were first interested in the distance between the sulfur atoms of the cysteine residues for the different peptides (100-ns simulation in water) (Figure 5 and Table 5). The purpose of this section is to get insight into the possible “spontaneous” DB formation. As reported in Table 5, the two peptides with the closest conformations are QS-13-1 and 5 as their average S–S distances are 0.7 ± 0.264 and 0.756 ± 0.277 nm, respectively. Then QS-13-4 and QS-13-3 display more elongated conformations (average distances between S atoms equal to 0.917 ± 0.275 and 0.926 ± 0.272 nm), and finally QS-13-2 seems to be the peptide least prone to bridge formation with an average distance of 1.113 ± 0.225 nm between sulfur atoms. Figure 5A–E allows us to visualize the distributions of the distance over time. Figure 5F recaps the occurrence of the distance for the different peptides. Four different profiles could be identified: the first type of distribution displays one peak of strong intensity at a distance of 0.5 nm and is associated with QS-13-1 and QS-13-5 peptides. The second type of distribution displays a slight shoulder around 0.5 nm as well as a rather flat profile between 0.5 and 1.5 nm. QS-13 and QS-13-4 peptides belong to this second type. The third type of profile, associated to QS-13-3, is characterized by two peaks of equivalent intensity. Finally, the last type of

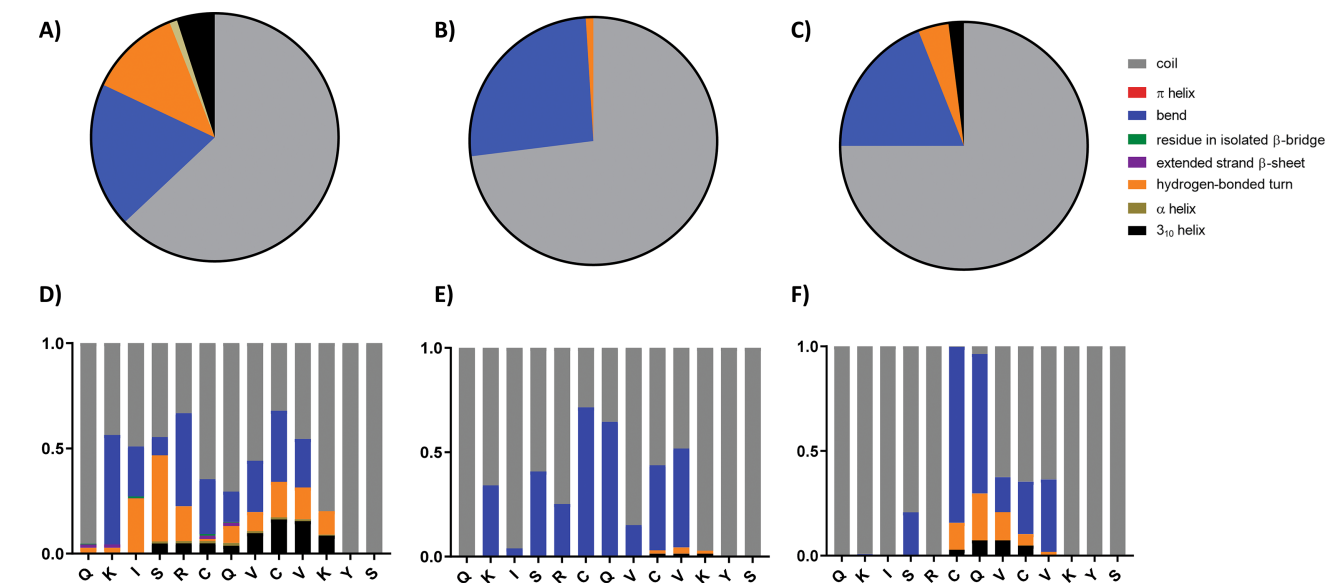


FIGURE 3 | Local secondary structure of QS-13 peptide. (A) Local structure of QS-13-w. (B) Local structure of QS-13-d. (C) Local structure of QS-13-DB-d. (D) Local structure propensity per residue of QS-13-w. (E) Local structure propensity per residue of QS-13-d. (F) Local structure propensity per residue of QS-13-DB-d.

TABLE 4 | The water solubility of QS-13 was increased by substituting the three most hydrophobic amino acids.

Peptide parameters	Sequence	Molecular weight (Da)	pI	Charge	Estimated half-life (h)
QS-13	QKISRCQVCVKYS	1541.85	9.39	+3	0.8
QS-13-1	QKSSRCQVCVKYS	1515.77	9.39	+3	0.8
QS-13-2	QKSSRCQGCGKYS	1431.60	9.39	+3	0.8
QS-13-3	QKGSRCQGCVKYS	1443.66	9.39	+3	0.8
QS-13-4	QKGSRCQGCGKYS	1401.58	9.39	+3	0.8
QS-13-5	QKGSRCQGCSKYS	1431.60	9.39	+3	0.8

Note: Table listing the sequence, the number of amino acids, the molecular weight, the pI, the charge, and the estimated half-life of QS-13 and substituted peptides.

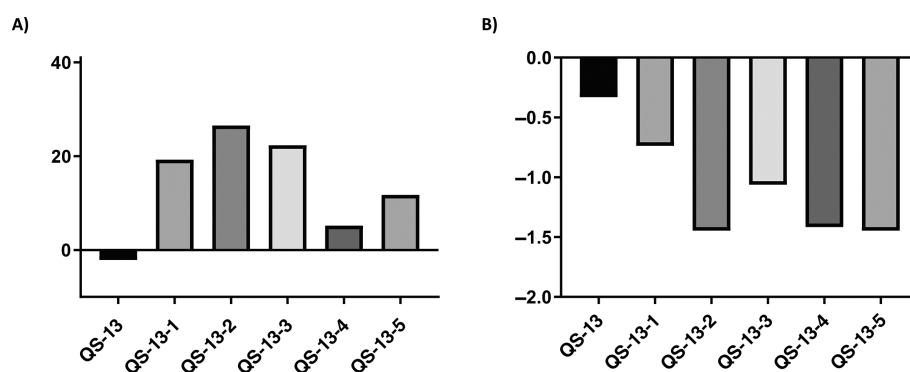


FIGURE 4 | Physicochemical parameters of the substituted peptides obtained from ProtParam. (A) Stability index. (B) GRAVY linked to the peptide hydrophobicity.

distribution displays one peak of strong intensity at a distance of 1.25 nm and is characteristic of QS-13-2.

In addition to the analysis of the distance between sulfur atoms of the cysteine residues, the distance between the alpha carbons of the C-ter and N-ter amino acids was also investigated.

The shortest average distance (1.030nm) is associated to the QS-13-3 peptide. The four other QS-13-derived peptides display similar values of average distances (from 1.219 to 1.248 nm). However, differences can be observed at the level of standard deviations. In comparison with the original QS-13 peptide, the five QS-13-derived peptides all display shorter end-to-end average

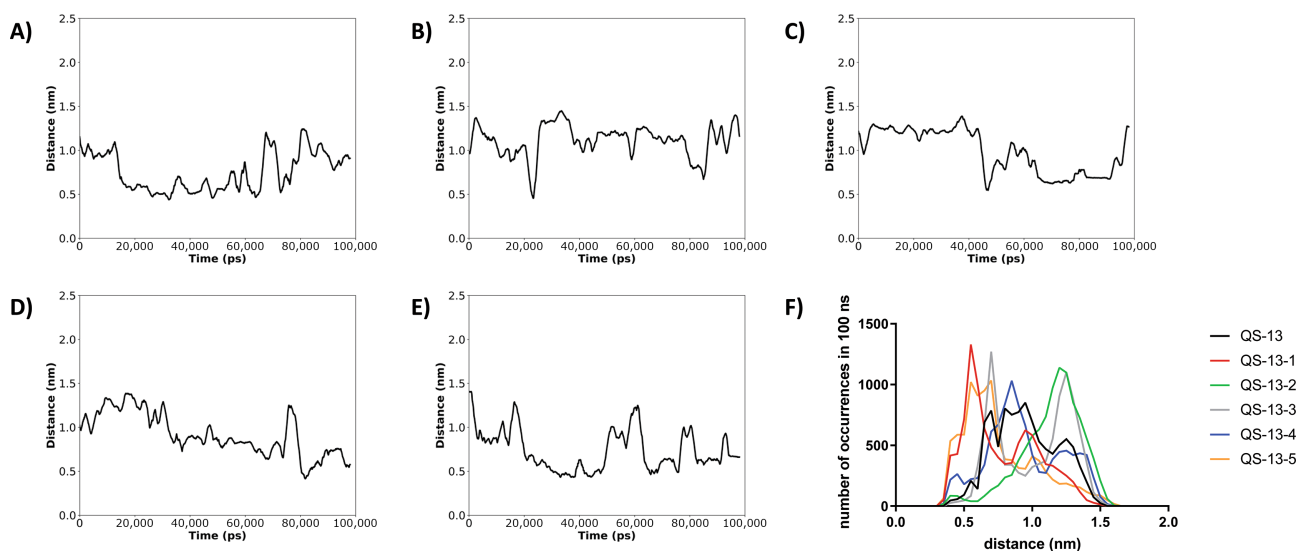


FIGURE 5 | Measurement of distances between the sulfur atoms from the cysteine residues in the substituted peptides. Time evolution of the distance between sulfur atoms from the cysteine residues of the different peptide (100 ns simulation) obtained from GROMACS. Distance between sulfur atoms from the cysteine residues over time in water for (A) QS-13-1, (B) QS-13-2, (C) QS-13-3, (D) QS-13-4, and (E) QS-13-5. (F) Occurrences according to sulfur atom distances (100-ns simulation). Values were obtained with a script on RStudio, with an interval of 0.05 nm.

TABLE 5 | Amino acid substitution could affect the disulfide bond formation of QS-13 derived peptides.

SSD	Average distance (nm)	Standard deviation (nm)
QS-13	0.926	0.236
QS-13-1	0.756	0.264
QS-13-2	1.113	0.225
QS-13-3	0.986	0.272
QS-13-4	0.917	0.275
QS-13-5	0.741	0.277

Note: Measurement of distances between sulfur atoms of the cysteine residues was performed using the gmx distance from GROMACS along the 100 ns of simulation.

distance (Table 6). The EED of the QS-13 peptide fluctuates quickly and explores short plateaus around the value of 1 nm (Figure 2A). Substituted peptides have somewhat the same profiles (Figure 6) except QS-13-3, which tends to stabilize around 1 nm during the second half of the MD simulation (Figure 6C). From the distributions of the EED computed from MD trajectories and using intervals of 0.05 nm, four types of profiles can be evidenced. QS-13 and QS-13-4 display a huge peak around 1.1 nm, while QS-13-1 displays a narrow peak around 0.75 nm and a small shoulder can be observed. The distribution profile of QS-13-3 is characterized by two peaks (0.8 and 1 nm). The profiles of QS-13-2 and QS-13-5 are characterized by three peaks (0.7, 0.9, and 1.2 nm).

For each substituted peptides with or without constrained DB, MD trajectories were analyzed using the DSSP algorithm. The average local secondary structures along the simulation were compiled (Figure 7). The main type of conformation adopted by the QS-13-derived peptides along the simulation are coil (in grey), bend (in blue), and turn (in orange) conformations. It can

TABLE 6 | Amino acid substitution could affect the end-to-end distance of QS-13-derived peptides.

EED	Average distance (nm)	Standard deviation (nm)
QS-13	1.357	0.523
QS-13-1	1.219	0.684
QS-13-2	1.248	0.563
QS-13-3	1.030	0.344
QS-13-4	1.219	0.374
QS-13-5	1.231	0.586

Note: Measurement of distances between the alpha carbon of glutamine and serine using gmx distance from GROMACS along the 100 ns of simulation.

be observed that the substitution of isoleucine and valine residue modulate mainly the “ordered” local secondary structures, in low amounts, such as bridges, sheets, and helices. The presence of the disulfide bond decreases the amount of coil structure or has almost no impact on this ratio, except in the case of QS-13-4, where coil structure increases when a disulfide bond is created. The ratio of bends is globally increased within the peptides upon disulfide bond presence and the ratio of turns is almost not modified, or, in two cases, decreased (QS-13-2 and QS-13-4). The creation of the disulfide bond decreased further the low amount of “ordered” local secondary structures. Two exceptions can be outlined: the ratio of β -bridges that increased in QS-13-4 (Figure 7D,I) and in QS-13-5 (Figure 7E,J).

To more accurately predict the impact of amino acid substitution, the local secondary structure was explored per residue over the whole 100-ns simulation in water for all the considered QS-13-derived peptides (Figure 8).

As previously observed (Figure 7), the analysis of the local secondary structure along the sequence clearly demonstrates the

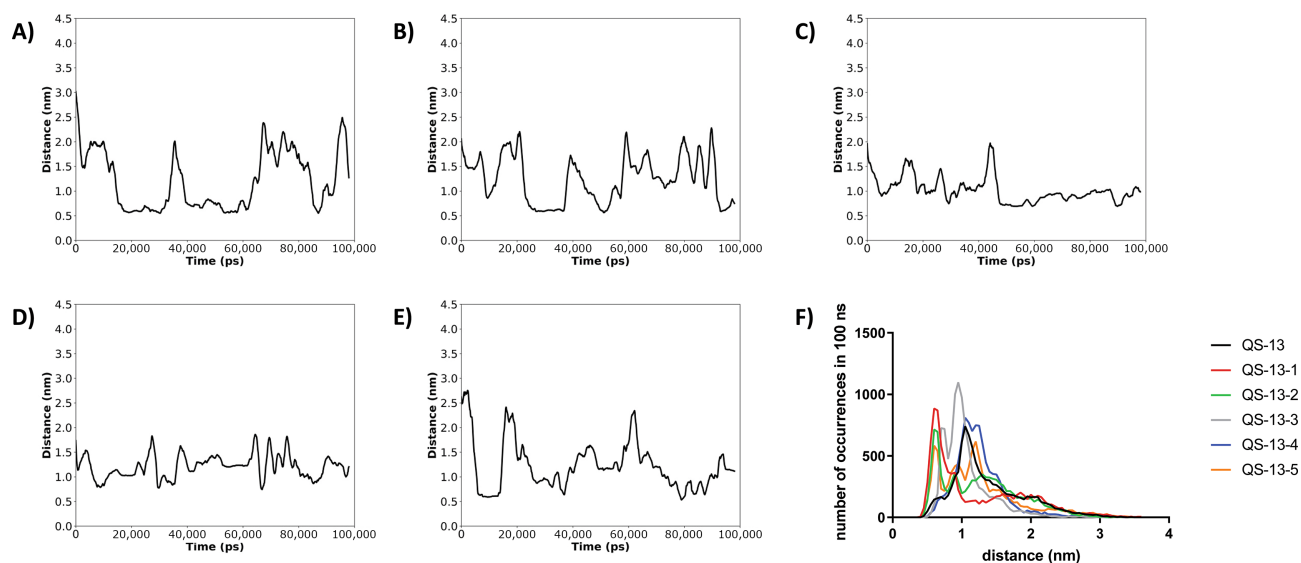


FIGURE 6 | Influence of peptide substitutions on their global structure. Time evolution of the distance between the alpha carbons of the glutamine and serine residues of the different peptides (100-ns simulation) obtained from GROMACS. Distance between alpha carbons of the glutamine and serine residues over time in water for (A) QS-13-1, (B) QS-13-2, (C) QS-13-3, (D) QS-13-4, and (E) QS-13-5. (F) Occurrences according to alpha carbons distances (100-ns simulation). Values were obtained with a script on RStudio, with an interval of 0.05 nm.

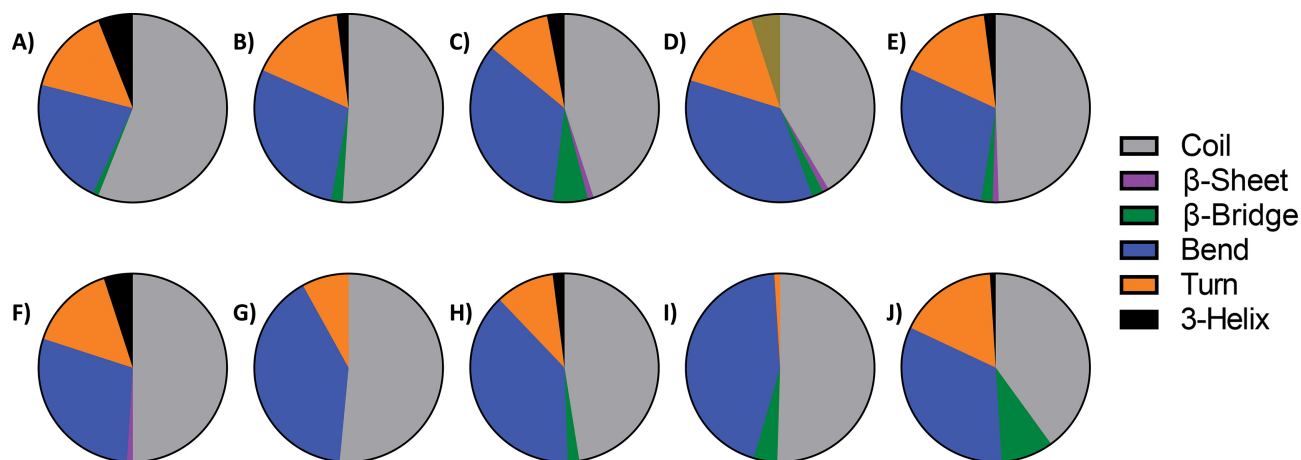


FIGURE 7 | Impact of hydrophobic amino acid substitution and disulfide bond creation on the average local secondary structure of the peptides. A DSSP analysis was performed on GROMACS and the ratios of local secondary structure obtained over a 100-ns simulation in water were calculated for peptides without (A, B, C, D, E) or with disulfide bond (F, G, H, I, J). (A and F) QS-13-1, (B and G) QS-13-2, (C and H) QS-13-3, (D and I) QS-13-4, and (E and J) QS-13-5.

predominance of coiled structures. Residues on the N-ter and C-ter parts of the peptides are mostly in coil structures: the first glutamine often presents around 50% of coil structures and the last tyrosine and serine residues are always seen in coil structures. QS-13-1 has mainly turns and bends in the center, with a helix on the outside. With the DB, the helix conformation in N-ter disappears, and the proportion of bends in the center increases (Figure 8A,F). QS-13-2 shows turns and bends in the center, and helix 3_{10} in N-ter. With the DB, the proportion of turns decreases and the proportion of bends increases. There are no more helices (Figure 8B,G). QS-13-3 without a DB has a lot of bends in the center and a small amount of residues in isolated beta bridges. With a DB, no drastic changes are observed (Figure 8C,H). QS-13-4 does not present a lot of bend shape but presents a short helix in the center of the peptide. In the

presence of a constrained DB, the proportion of bend strongly increases in the center of the peptide (Figure 8D,I). Without the DB, QS-13-5 has less bend in the center than with the DB. The bend conformation is shifted toward the N-terminal without DB (Figure 8E,J).

Further characterization through Ramachandran plot (Figure 9) and clustering (Figure 10) analysis were performed.

The propensity of any residue within the peptide to explore a conformation (characterized by a pair of ϕ , ψ dihedral angle values) during the MD trajectory appears as colored “spots” ranging from white (medium propensity) to red (high propensity) in the Ramachandran diagrams of Figure 9. The observation of these diagrams associated with modified QS-13 peptides in

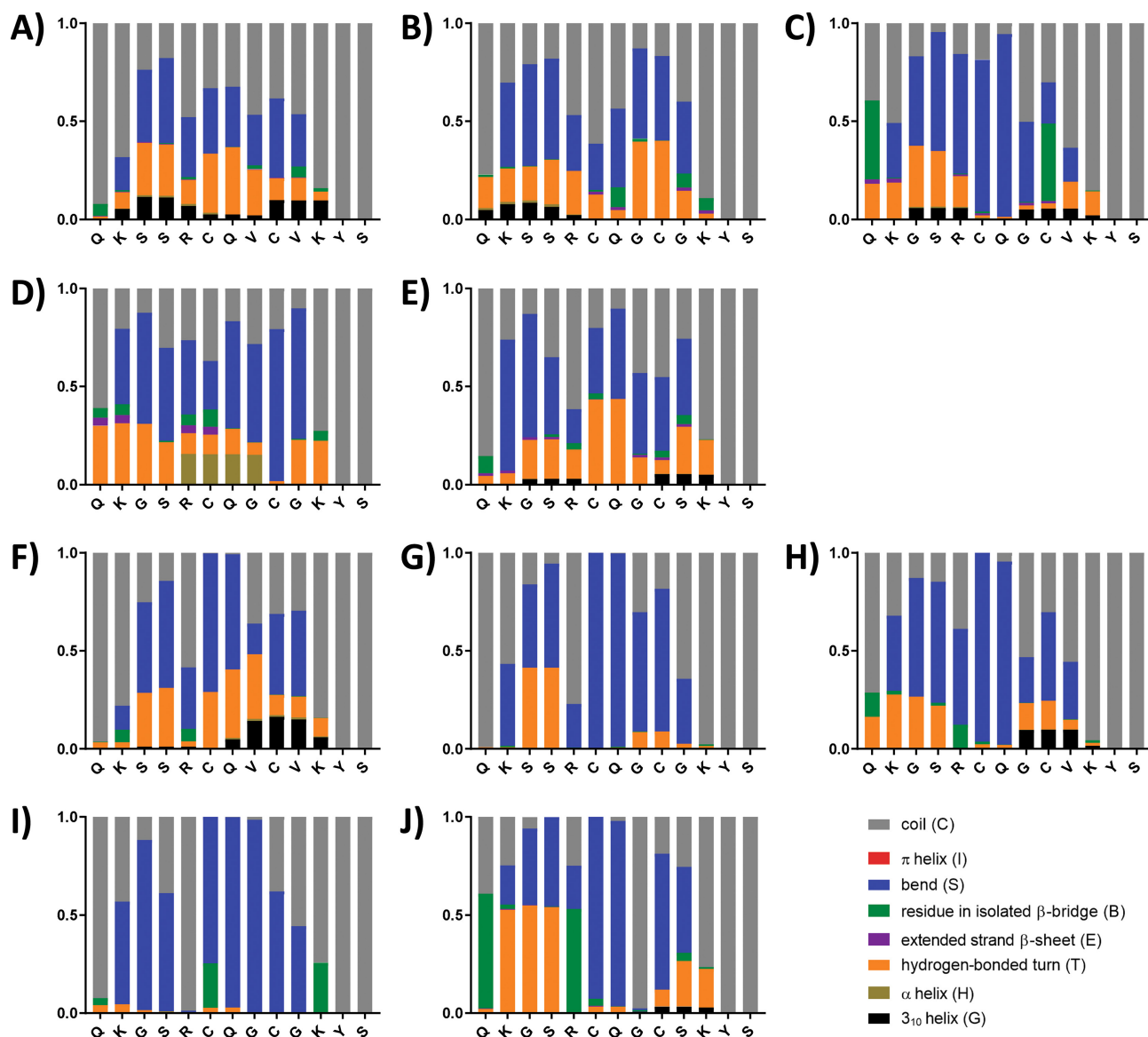


FIGURE 8 | Impact of hydrophobic amino acid substitution and disulfide bond creation on the local secondary structure. Local secondary structure assignment was performed using GROMACS and the DSSP algorithm applied to 100-ns simulation in water for peptides without (A, B, C, D, E) or with disulfide bond (F, G, H, I, J). (A and F) QS-13-1, (B and G) QS-13-2, (C and H) QS-13-3, (D and I) QS-13-4, and (E and J) QS-13-5.

aqueous solvent clearly reveals a singular mark that can be associated with a fingerprint, characterized by four spots located in the upper left-hand part of the diagram. The appearance of white spots on the right-hand side of the diagrams is clearly linked to the glycine content: no spots are observed in the diagrams associated to the QS-13-1 peptide (Figure 9A,F), which is the only one to contain no glycine. Upon the presence of the DB, the relative intensity of the four spots characteristic of a peptide derived from QS-13 is globally diminished, with the occasional disappearance of the red color associated with certain peaks, reflecting reduced exploration of the associated conformations.

From the patterns observed in Figure 8, it seems reasonable to apply clustering analysis to the trajectories to identify the main representative conformations of the QS-13-derived peptides. Figure 10 presents the conformations obtained using the gromos clustering algorithm applied to the backbone with a cutoff of 3 Å. Adding a DB to QS-13-1 did not alter the

global shape (Figure 10A,F). Adding a DB to QS-13-2 significantly flattened the structure compared with the conformation without a DB (Figure 10B,G). Adding a DB to QS-13-3 did not modify the conformation (Figure 10C,H). Adding a DB to QS-13-4 drastically altered the conformation, transitioning from a twisted structure to one similar to QS-13-1 and QS-13-1 with a DB (Figure 10D,I). Adding a DB did not modify the structure of QS-13-5 (Figure 10E,F). Overall, two main conformations are evident: a twisted, spring-like structure (Figure 10D,G) and structures more W-shaped (Figure 10A,B,F,I), with some structures being a hybrid of the two (Figure 10C,E,H,J).

3.3 | Anti-Migratory Effect of QS-13 3 Peptide on Melanoma Cells

Among the various peptides studied above, as a proof of concept, we selected the QS-13-3 peptide, which presents only two

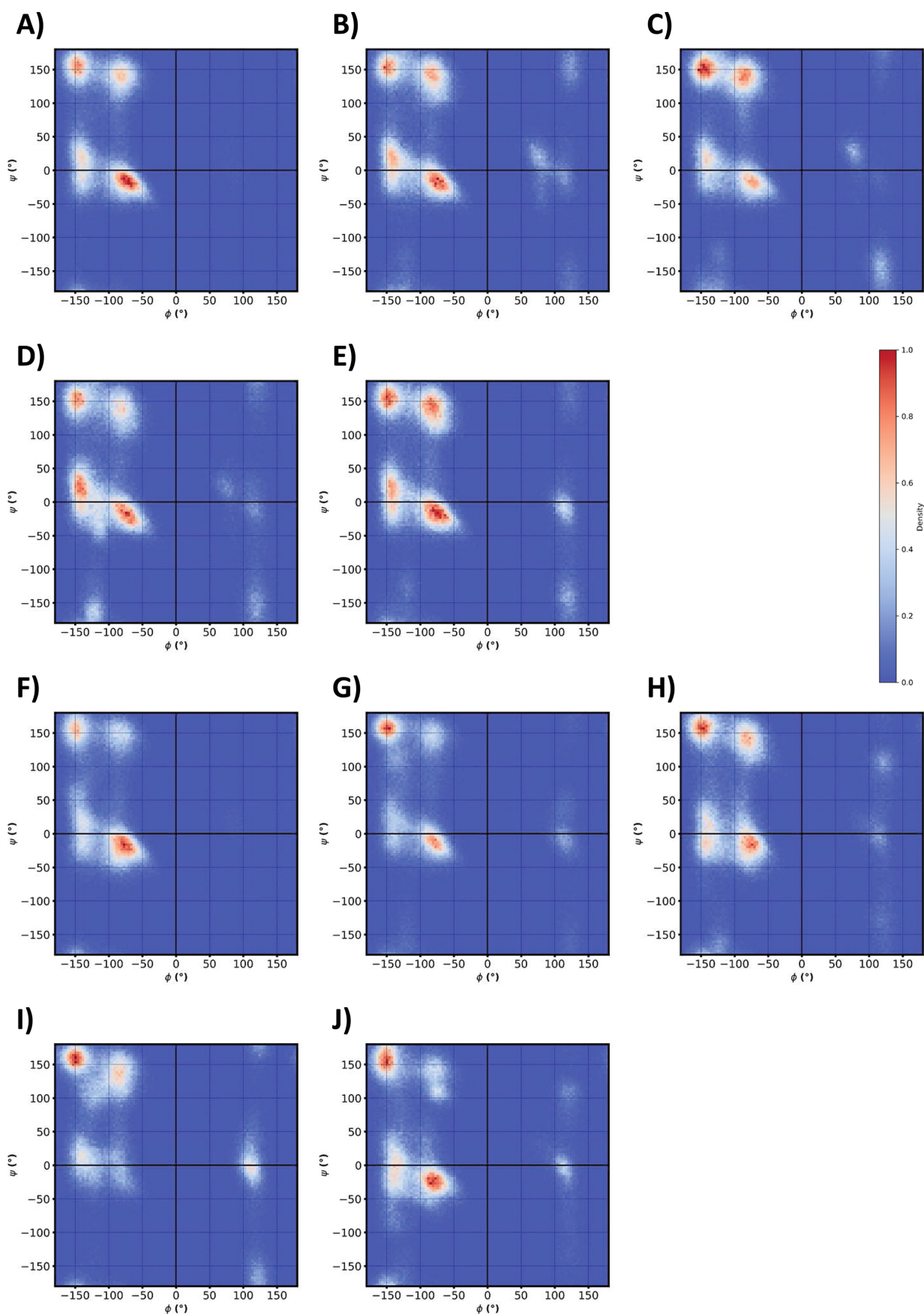


FIGURE 9 | Stereochemical characterization of peptide conformations using Ramachandran plots. Ramachandran plots were generated processing each trajectory with GROMACS for peptides without (A, B, C, D, E) or with disulfide bond (F, G, H, I, J). (A and F) QS-13-1, (B and G) QS-13-2, (C and H) QS-13-3, (D and I) QS-13-4, and (E and J) QS-13-5.

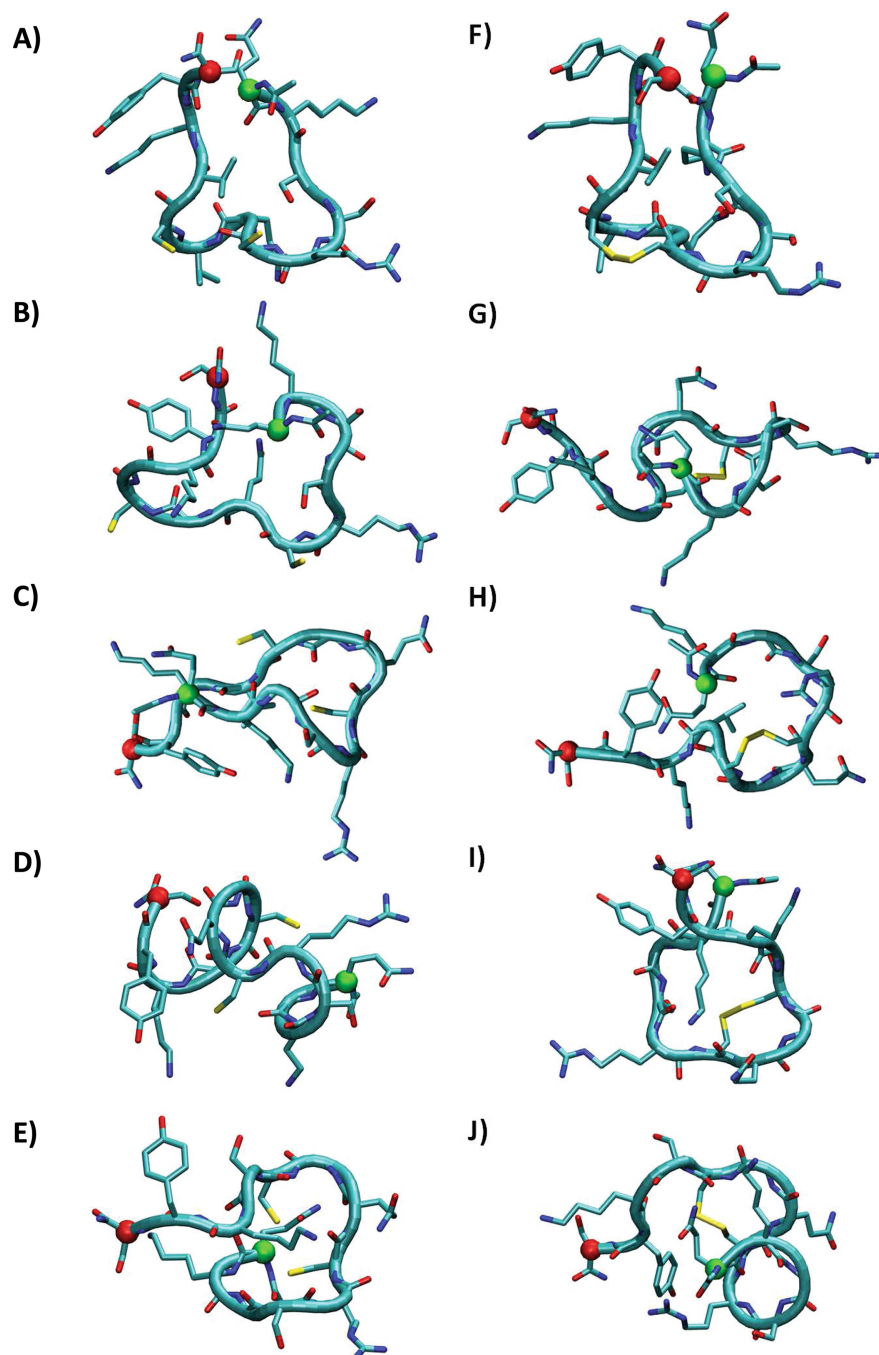


FIGURE 10 | Most representative conformations of substituted peptides in water. Molecular dynamics simulations were performed using gromos clustering algorithm for peptides without (A, B, C, D, E) or with disulfide bond (F, G, H, I, J). (A and F) QS-13-1, (B and G) QS-13-2, (C and H) QS-13-3, (D and I) QS-13-4, and (E and J) QS-13-5.

substituted amino acids, the highest stability index as well as a high hydropathicity index. The QS-13-3 peptide, synthesized by Proteogenix, was fully soluble in culture media and did not precipitate even after hours (Figure S1C), unlike original QS-13 peptide, which precipitated within 2 h if directly solubilized in culture medium (Figure S1D). We previously demonstrated the anti-migratory effect of QS-13 on melanoma cells [2]. The effect of QS-13-3 peptide was compared to that of the QS-13 peptide at the same concentration (40 μ M) on HT-144 melanoma cell migration. It was at least as effective as the original peptide (Figure 11).

4 | Discussion and Conclusion

As reported in Section 1, the NC1 domain of the alpha 4 chain of type IV collagen exerts antitumor properties in a melanoma model and inhibits angiogenesis [1]. The minimal active sequence identified to date comprises 13 amino acids: QKISRCQVCVKYS [2, 3]. Unfortunately, although presenting a hydropathicity index of -0.3331 (determined using the ProtParam tool), this peptide is not soluble in aqueous media and requires prior dissolution in DMSO. Once in solution in a culture medium containing 0.2% DMSO, the peptide spontaneously forms a DB between the two

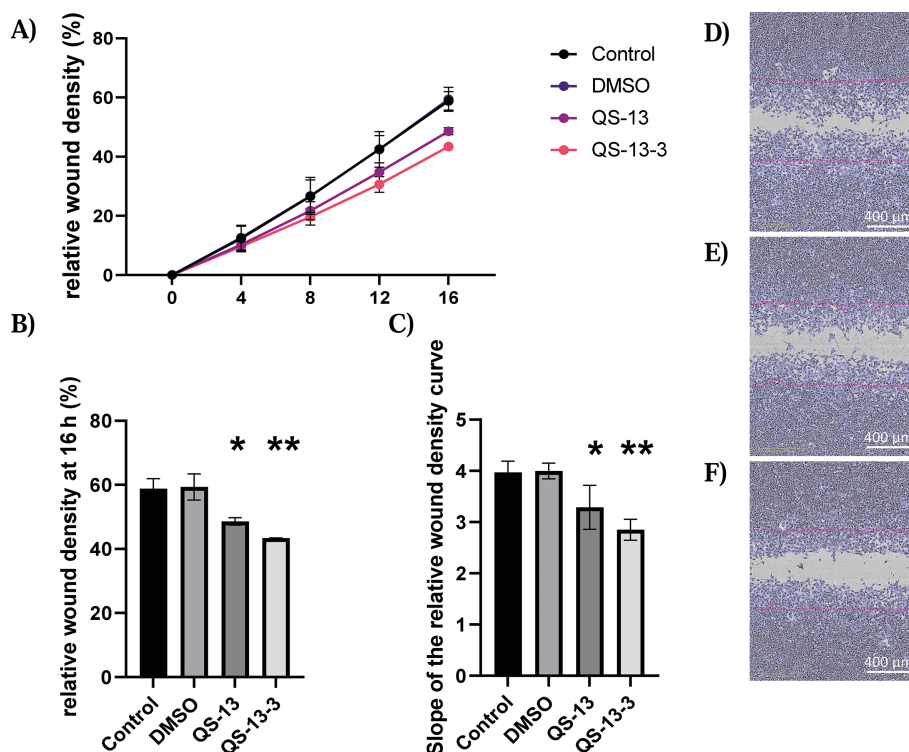


FIGURE 11 | Impact of QS-13 and QS-13-3 peptides on melanoma cell migration in a wound healing model. Kinetics of HT144 cell migration monitored over 16 h, represented as relative wound density (A). Histogram showing the percentage of wound closure at 16 h (B). Histogram illustrating the direction coefficient of the migration curves between 4 and 16 h (C). Representative images acquired after 16 h for the control condition without peptide (D), with the QS-13 peptide pre-solubilized in DMSO (E), with the QS-13-3 peptide directly solubilized in the culture medium (F). Histograms represent the mean \pm SD of two independent experiments with $n = 8$ biological replicates. * $p < 0.05$, ** $p < 0.01$.

cysteine residues, as demonstrated by mass spectroscopy analysis [2]. The substitution of one or the other of these two residues prevents its binding to the receptor [1].

We were therefore interested in investigating the structural properties of this peptide in the presence of DMSO or water.

A decrease in the average distance between the sulfur atoms of cysteine residues was observed in DMSO compared with water. The distribution of the S–S distance showed a high population with a very small distance between sulfur atoms in DMSO, leading to an increased probability of intrachain DB formation. However, in water, the DB has the possibility of forming, but with a lower probability than in DMSO. We can conclude that DMSO seems to promote DB formation, a key element in peptide binding to its receptor and, consequently, in its biological activity. The ability of DMSO to promote DB formation has been reported previously [33].

DMSO also tends to move away the ends of the peptide. As QS-13 tends to present a bend conformation in the center, this suggests that the peptide could adopt a horseshoe conformation in water, and an omega conformation in DMSO, despite the presence of an intrachain DB.

The bend conformation appears essential for the biological function of the QS-13 peptide [2]; even if DMSO seems to favor this conformation, it is nevertheless observed in the three considered conditions in the context of this study (peptide with or without

constrained DB in DMSO or without constrained DB in water), therefore including aqueous solvent, which is a good omen. DMSO has been used as a commercial solvent since 1953, while the history of DMSO as a pharmaceutical began in 1961. Since then, it has been frequently used as a diluent in biological studies and as a vehicle for drug therapy, as well as in the in vivo administration of water-insoluble substances [34]. However, the use of DMSO is not optimal for the development of new therapeutic strategies as it affects cellular pathways [31, 34].

The solubility of QS-13 in aqueous media can be improved using hydrophobic residue substitution. Mutating isoleucine residue and combination of valine residues, the predicted stability of the peptide was modified, which is not necessarily a problem as long as the stability index keeps a value lower than 40. The substituted peptides were then still considered stable. GRAVY values indicate that the peptides may be soluble in aqueous media without prior DMSO solubilization, unlike the original QS-13 peptide.

Results from Figure 5 indicate that all the candidates may form (with more or less propensity) DBs. Some peptides, such as QS-13-1 and 5, display profiles that clearly favor conformation with a distance between the two cysteine residues close to 0.5 nm. Other peptides display profiles that are globally associated to distance between sulfur atoms that will less favor the formation of bridges (QS-13-2 and 4). The remaining peptide (QS-13-3) adopts two distinct conformations. Additionally, time evolutions of the distance between sulfur atoms provide

additional information regarding the stability of conformations and the speed of transition between conformations.

The EED, in terms of average values and in terms of distribution profile, allow making distinctions between different groups of peptides that can present more and less tight or elongated conformations.

To go through a more thorough characterization of the peptide structure, the local secondary structure analysis was of interest. Independently of the amino acid substitutions and/or the presence of a disulfide bond, the three main local secondary structures are coils, bends, and turns. The presence of the disulfide bond increases the bend conformations, whereas the amount of coils and turns decrease. Particularly, a high proportion of bend conformation located in the middle of the peptide, around the active site encompassing the two cysteine residues, was observed upon the presence of the DB. This conformation seems crucial to the structure–function relationship of the peptide. It is clear that the formation of a DB affects the structure of the different peptides. When no disulfide bond is imposed, it could be observed that amino acid substitution impacts the overall structure, increasing slightly the amount of “ordered” local secondary structure.

Finally, Ramachandran diagrams not only allowed us to verify that acceptable conformations were adopted by the modified peptides but also allowed the identification of a fingerprint patterns and spots associated with the presence of glycine residues.

Although the behaviors and structures are sometimes different, most of the structural properties are preserved in the substituted peptides.

As a proof of concept, the QS-13-3 peptide, which contains two substituted amino acids, exhibits highest stability index, and has a low hydropathicity index, was synthesized. It was fully soluble and did not precipitate even after hours.

We previously reported the anti-migratory effect of QS-13 on melanoma cells [2]. The effect of QS-13-3 peptide was compared with that of the QS-13 peptide at the same concentration (40 μ M) on melanoma cell migration in a wound healing model. It was at least as effective as the original peptide, in accordance with in silico studies.

These results are encouraging for the development of new therapeutic strategies based on QS-13-derived peptides.

Acknowledgments

This work was supported by the Région Champagne-Ardenne, the Université de Reims Champagne Ardenne, the Ligue Contre le Cancer (Conférence de Coordination Inter Régionale du Grand Est: CCIR-GE), the Centre Nationale de la Recherche Scientifique, and the ITMO Cancer Aviesan within the framework of the 2021-2030 Cancer Control Strategy, on funds administered by Insem (N°23CQ006-00). The authors thank the HPC-Regional Center ROMEO, the Multiscale Molecular Modeling Platform (P3M) of the University of Reims Champagne-Ardenne (France), for providing time and support. Vivien Paturel is a

PhD fellow funded by Région Champagne-Ardenne and Université de Reims Champagne Ardenne.

Conflicts of Interest

The authors declare no conflicts of interest.

Data Availability Statement

The data that support the findings of this study are available from the corresponding author, Dr Sylvie BRASSART-PASCO, upon reasonable request. The script used to Ramachandran diagrams generation is accessible from GitHub: https://github.com/vivienpaturel/Ramachandran-plot-from-XVG-file-GROMACS---python3/blob/main/script_ramachandran.py.

References

1. S. Brassart-Pasco, K. Sénéchal, J. Thevenard, et al., “Tetrastatin, the NC1 Domain of the α 4(IV) Collagen Chain: A Novel Potent Anti-Tumor Matrikine,” *PLoS One* 7, no. 4 (2012): e29587.
2. E. Lambert, E. Fuselier, L. Ramont, et al., “Conformation-Dependent Binding of a Tetrastatin Peptide to α v β 3 Integrin Decreases Melanoma Progression Through FAK/PI3K/Akt Pathway Inhibition,” *Scientific Reports* 8 (2018): 9837.
3. A. Vautrin-Glabik, J. Devy, C. Bour, et al., “Angiogenesis Inhibition by a Short 13 Amino Acid Peptide Sequence of Tetrastatin, the α 4(IV) NC1 Domain of Collagen IV,” *Frontiers in Cell and Development Biology* 8 (2020): 775.
4. S. Tunçer, R. Gurbanov, I. Sheraj, E. Solel, O. Esenturk, and S. Banerjee, “Low Dose Dimethyl Sulfoxide Driven Gross Molecular Changes Have the Potential to Interfere With Various Cellular Processes,” *Scientific Reports* 8, no. 1 (2018): 14828.
5. A. Vishnyakov, A. P. Lyubartsev, and A. Laaksonen, “Molecular Dynamics Simulations of Dimethyl Sulfoxide and Dimethyl Sulfoxide–Water Mixture,” *The Journal of Physical Chemistry A* 105, no. 10 (2001): 1702–1710.
6. D. Van der Spoel and H. J. Berendsen, “Molecular Dynamics Simulations of Leu-Enkephalin in Water and DMSO,” *Biophysical Journal* 72, no. 5 (1997): 2032–2041.
7. I. Demetropoulos, A. Tsibiris, V. Tsikaris, M. Sakarellos-Daitsiotis, and C. Sakarellos, “Conformational Properties of the Arg-Leu-Gly Tripeptide–DMSO–Water Clusters With the Combined Use of Molecular Dynamics and Energy Minimization Studies,” *Journal of Biomolecular Structure & Dynamics* 12, no. 4 (1995): 755–765.
8. H. Cui, M. Vedder, U. Schwaneberg, and M. D. Davari, “Using Molecular Simulation to Guide Protein Engineering for Biocatalysis in Organic Solvents,” *Methods in Molecular Biology* 2397 (2022): 179–202.
9. J. Karjalainen, H. Henschel, M. J. Nissi, M. T. Nieminen, and M. Hanni, “Dipolar Relaxation of Water Protons in the Vicinity of a Collagen-Like Peptide,” *The Journal of Physical Chemistry B* 126, no. 13 (2022): 2538–2551, <https://doi.org/10.1021/acs.jpcc.2c00052>.
10. M. L. Sforça, S. Oyama, Jr., F. Canduri, et al., “How C-Terminal Carboxyamidation Alters the Biological Activity of Peptides From the Venom of the Eumenine Solitary Wasp,” *Biochemistry* 43, no. 19 (May 2004): 5608–5617, <https://doi.org/10.1021/bi0360915>.
11. Y. Ma, Y. Wu, and L. Li, “Relationship Between Primary Structure or Spatial Conformation and Functional Activity of Antioxidant Peptides From *Pinctada fucata*,” *Food Chemistry* 264 (2018): 108–117.
12. K. Bozovičar and T. Bratkovič, “Small and Simple, Yet Sturdy: Conformationally Constrained Peptides With Remarkable Properties,” *International Journal of Molecular Sciences* 22, no. 4 (2021): 1611.

13. M. B. Dewal and S. M. Firestine, "Non-Peptidic α -Helical Mimetics as Protein-Protein Interaction Inhibitors," *Current Medicinal Chemistry* 18, no. 16 (2011): 2420–2428.
14. "GROMACS," 3 Manual, Accessed May 27, 2023, <https://zenodo.org/records/10017699>.
15. D. Van Der Spoel, E. Lindahl, B. Hess, G. Groenhof, A. E. Mark, and H. J. C. Berendsen, "GROMACS: Fast, Flexible, and Free," *Journal of Computational Chemistry* 26, no. 16 (2005): 1701–1718.
16. W. Kabsch and C. Sander, "Dictionary of Protein Secondary Structure: Pattern Recognition of Hydrogen-Bonded and Geometrical Features," *Biopolymers* 22, no. 12 (1983): 2577–2637.
17. L. K. Mosavi and Z. Y. Peng, "Structure-Based Substitutions for Increased Solubility of a Designed Protein," *Protein Engineering* 16, no. 10 (2003): 739–745.
18. E. Gasteiger, C. Hoogland, A. Gattiker, et al., "Protein Identification and Analysis Tools on the ExPASy Server," in *The Proteomics Protocols Handbook*, ed. J. M. Walker (Totowa, NJ: Humana Press, 2005), 571–607, <https://doi.org/10.1385/1-59259-890-0:571>.
19. R. Trivedi and H. A. Nagarajaram, "Substitution Scoring Matrices for Proteins—An Overview," *Protein Science* 29, no. 11 (2020): 2150–2163.
20. G. N. Ramachandran, C. Ramakrishnan, and V. Sasisekharan, "Stereochemistry of Polypeptide Chain Configurations," *Journal of Molecular Biology* 7, no. 1 (1963): 95–99.
21. W. Humphrey, A. Dalke, and K. Schulten, "VMD: Visual Molecular Dynamics," *Journal of Molecular Graphics* 14, no. 1 (1996): 33–38.
22. W. L. Jorgensen, D. S. Maxwell, and J. Tirado-Rives, "Development and Testing of the OPLS All-Atom Force Field on Conformational Energetics and Properties of Organic Liquids," *Journal of the American Chemical Society* 118, no. 45 (1996): 11225–11236.
23. W. L. Jorgensen, and J. D. Madura, "Quantum and Statistical Mechanical Studies of Liquids. 25. Solvation and Conformation of Methanol in Water," *Journal of the American Chemical Society* 105, no. 6 (1983): 1407–1413.
24. B. Hess, H. Bekker, H. J. C. Berendsen, and J. G. E. M. Fraaije, "LINCS: A Linear Constraint Solver for Molecular Simulations," *Journal of Computational Chemistry* 18, no. 12 (1997): 1463–1472.
25. G. Bussi, D. Donadio, and M. Parrinello, "Canonical Sampling Through Velocity Rescaling," *The Journal of Chemical Physics* 126, no. 1 (2007): 014101.
26. U. Essmann, L. Perera, M. Berkowitz, T. Darden, H. Lee, and L. Pedersen, "A Smooth Particle Mesh Ewald Method," *The Journal of Chemical Physics* 103 (1995): 8577–8593.
27. M. Parrinello and A. Rahman, "Polymorphic Transitions in Single Crystals: A New Molecular Dynamics Method," *Journal of Applied Physics* 52, no. 12 (1981): 7182–7190.
28. B. Brigida Bochicchio, A. Pepe, M. Crudele, N. Belloy, S. Baud, and M. Dauchez, "Tuning Self-Assembly in Elastin-Derived Peptides," *Soft Matter* 11 (2015): 3385–3395.
29. J. Oudart, M. Dou , A. Vautrin, et al., "The Anti-Tumor NC1 Domain of Collagen XIX Inhibits the FAK/PI3K/Akt/mTOR Signaling Pathway Through $\alpha\beta3$ Integrin Interaction," *Oncotarget* 7 (2016): 1516–1528.
30. J. Dauv , N. Belloy, R. Rivet, et al., "Differential MMP-14 Targeting by Lumican-Derived Peptides Unraveled by In Silico Approach," *Cancers* 13, no. 19 (2021): 4930.
31. J. Kyte and R. F. Doolittle, "A Simple Method for Displaying the Hydropathic Character of a Protein," *Journal of Molecular Biology* 157, no. 1 (1982): 105–132.
32. T. M. Abramyan, J. A. Snyder, A. A. Thyparambil, S. J. Stuart, and R. A. Latour, "Cluster Analysis of Molecular Simulation Trajectories for Systems Where Both Conformation and Orientation of the Sampled States Are Important," *Journal of Computational Chemistry* 37, no. 21 (2016): 1973–1982.
33. J. P. Tam, C. R. Wu, W. Liu, and J. W. Zhang, "Disulfide Bond Formation in Peptides by Dimethyl Sulfoxide. Scope and Applications," *Journal of the American Chemical Society* 113, no. 17 (1991): 6657–6662.
34. M. Moskot, J. Jak bkiewicz-Banecka, A. Kloska, E. Piotrowska, M. Narajczyk, and M. Gabig-Cimi ska, "The Role of Dimethyl Sulfoxide (DMSO) in Gene Expression Modulation and Glycosaminoglycan Metabolism in Lysosomal Storage Disorders on an Example of Mucopolysaccharidosis," *International Journal of Molecular Sciences* 20, no. 2 (2019): 304.

Supporting Information

Additional supporting information can be found online in the Supporting Information section.